Molecular Origins of Friction: The Force on Adsorbed Layers

Marek Cieplak; Elizabeth D. Smith; Mark O. Robbins

Science, New Series, Vol. 265, No. 5176 (Aug. 26, 1994), 1209-1212.

12. J. F. Stebbins, I. Farnan, E. H. Williams, J. Roux, *Phys. Chem. Miner.* **16**, 763 (1989).
13. D. R. Spearing, I. Farnan, J. F. Stebbins, *ibid.* **19**, 307 (1992).
14. D. R. Spearing, J. F. Stebbins, I. Farnan, *Am. Mineral.*, in press.
15. Spectra were collected with a modified Varian VXR400S spectrometer at a resonant frequency of 79.5 MHz for ^{29}Si and with a high-temperature MAS probe from Doty Scientific. We used 90° pulse lengths of 10.5 μs and spinning rates of 3 to 4.5 kHz. Temperatures were calibrated by spinning an empty sample container with an inserted thermocouple in the probe at high temperature. Delay times between radio-frequency pulse trains were selected after measurement of spin-lattice relaxation times to avoid saturation effects. The 2D spectra shown took 1 to 2 hours each to collect. The abundance of SiO_5 groups is too small, unfortunately, to directly test the involvement of this species in exchange (*30*). The $K_2Si_4O_9$ glass was synthesized from 95% ^{29}Si-enriched SiO_2 and K_2CO_3 as described previously (*4*) and was doped with 0.2 weight % CoO to accelerate spin-lattice relaxation.
16. Exchange rates were derived by plotting the natural logarithm of the ratios of the intensities of the exchange and Q^4 peaks in the slices shown in Fig. 4 versus mixing time. If (as is the case for this sample) spin-lattice relaxation times are long when compared to t_{mix}, the slope of this plot is equal to the exchange rate $1/\tau_{exchange}$ (*10*). The estimated uncertainties include errors in this fit as well as in intensities.
17. In calculating viscosity from the observed exchange times, we chose $d = 0.31$ nm as a typical Si-Si distance and $a = 0.04$ nm as the radius of the Si cation. For both models, the Einstein-Smoluchowski equation ($D = d^2/2\tau$) is chosen to relate diffusivity to jump time (*31*). For the Eyring model, $\eta = k_BT/(dD)$; for the Stokes-Einstein model, $\eta = k_BT/(6\pi aD)$. The simple statistical character of these equations cannot be expected to reproduce the details of a complex, partially ionic, partially covalently bonded liquid, but they are nonetheless useful starting points.
18. The solid line in Fig. 5 results from a fit to published data both at relatively high temperature (*32*) and near to T_g (*33*), with $\log \eta = -2.654 + 5069/(T - 423.4)$, with T in kelvins and η in pascal seconds. This predicts other fiber elongation rates to within 0.15 log units (*34*). We observed the glass transition behavior of our NMR sample of $K_2Si_4O_9$ directly using a Dupont 2100 differential scanning calorimeter. After cooling at 20°C/s and heating at the same rate, we recorded an onset temperature of 490° ± 2°C and a peak temperature of 534° ± 2°C. Our fit equation for viscosity predicts $\log \eta = 12.3$ and 10.6 (Pa · s) at these temperatures. A dilatometric value of T_g of 500°C, at which point $\log \eta$ is typically 12.0 (Pa · s), has been reported (*5*).
19. G. W. Scherer, *Relaxation in Glass and Composites* (Wiley, New York, 1986).
20. C. A. Angell, *J. Non-Cryst. Solids* **131–133**, 13 (1991).
21. D. B. Dingwell and S. L. Webb, *Eur. J. Mineral.* **2**, 427 (1990).
22. K. L. Ngai, R. W. Rendell, A. K. Rajagopal, S. Teitler, *Ann. N.Y. Acad. Sci.* **484**, 150 (1986).
23. N. Shimizu and I. Kushiro, *Geochim. Cosmochim. Acta* **48**, 1295 (1984).
24. S. Sen and J. F. Stebbins, *Phys. Rev. B*, in press.
25. B. T. Poe *et al.*, *J. Phys. Chem.* **96**, 8220 (1992).
26. P. Fiske and J. F. Stebbins, *Am. Mineral.*, in press.
27. J. F. Stebbins and I. Farnan, *Science* **255**, 586 (1992).
28. B. Coté, D. Massiot, F. Taulelle, J. Coutures, *Chem. Geol.* **96**, 367 (1992).
29. S. Shimokawa *et al.*, *Chem. Lett.* **1990**, 617 (1990).
30. J. F. Stebbins, *Nature* **351**, 638 (1991).
31. P. W. Atkins, *Physical Chemistry* (Freeman, New York, 1986).
32. L. Shartsis, S. Spinner, W. Capps, *J. Am. Ceram. Soc.* **35**, 155 (1952).
33. S. L. Webb and D. B. Dingwell, *Phys. Chem. Miner.* **17**, 125 (1990).
34. O. V. Mazurin, M. V. Streltsina, T. P. Shvaiko-Shvaikovskaya, *Silica Glass and Binary Silicate Glasses* (Elsevier, New York, 1983).
35. This work was supported by National Science Foundation grants EAR 8905188 and EAR 9204458. We thank the two anonymous reviewers for insightful and helpful comments.

28 April 1994; accepted 12 July 1994

Molecular Origins of Friction: The Force on Adsorbed Layers

Marek Cieplak,* Elizabeth D. Smith, Mark O. Robbins†

Simulations and perturbation theory are used to study the molecular origins of friction in an ideal model system, a layer of adsorbed molecules sliding over a substrate. These calculations reproduce several surprising features of experimental results. In most cases, the frictional force on a solid monolayer has a different form from that observed between macroscopic solids. No threshold force or static friction is needed to initiate sliding; instead, the velocity is proportional to the force. As in experiments, incommensurate solid layers actually slide more readily than fluid layers. A comparison of experiment, simulation, and analytic results shows that dissipation arises from anharmonic coupling between phonon modes and substrate-induced deformations in the adsorbate.

Friction plays a key role in holding our buildings and clothes together, determining the function and failure of our machines, and allowing us to sense the outside world. However, our understanding of the molecular origins of this force is relatively primitive. The goal of this report is to provide a detailed molecular description of friction in an ideal model system, a layer of molecules adsorbed on a solid substrate.

The frictional force between macroscopic solids is normally described by phenomenological laws. Fluid dynamics implies that the friction F for a lubricated contact is proportional to the relative velocity v of the solids. We will refer to this linear velocity dependence as "viscous" friction. The behavior of dry contacts is normally very different. A static frictional force F_{stat} must be exceeded to initiate sliding, and there is a smaller kinetic friction F_{kin} between sliding solids that is only weakly dependent on v. We will refer to this type of behavior as "static" friction.

New experimental methods have made it possible to study friction in single contacts of well-defined area. The results are often strikingly different from those expected from macroscopic laws. For example, static friction and stick-slip motion are observed in lubricated contacts when the film thickness becomes comparable to molecular dimensions (*1*, *2*). Recent simulations indicate that this unusual behavior is due to solidification of the lubricant by the confining solid walls (*3*, *4*).

Experimental studies of the frictional force between a substrate and an adsorbed monolayer also produce surprising results (*5*, *6*). Crystalline layers exhibit viscous rather than static friction laws. Indeed, crystalline monolayers slide more readily than fluid monolayers. The measured forces for both phases are smaller by roughly three orders of magnitude than expected from the bulk viscosity of the adsorbed phase. We show here that these counterintuitive results can be reproduced by simulations and perturbation theory. These calculations provide a quantitative description of the frictional force in terms of the excitation and subsequent decay of phonon modes in the adsorbed film.

Most experimental studies of the frictional force on adsorbed films have used noble gas atoms adsorbed on the (111) surfaces of noble metal substrates (Au or Ag) (*5*–*7*). The equilibrium properties of these systems have been extensively studied by researchers interested in two-dimensional phase transitions (*8*). Because the substrate is much more rigid than the adsorbate, the displacement of substrate molecules from ideal lattice sites is usually ignored. The substrate then produces a fixed periodic potential that acts on the adsorbed layer. We made this approximation in most of our calculations and discuss its limitations below.

The interactions between noble gas adsorbate atoms are well described by a Lennard-Jones potential

$$V(r) = 4\varepsilon[(\sigma/r)^{12} - (\sigma/r)^6] \qquad (1)$$

where r is the atomic separation and ε and σ are characteristic energy and length

Department of Physics and Astronomy, Johns Hopkins University, Baltimore, MD 21218, USA.

*On leave from the Institute of Physics, Polish Academy of Sciences, 02-668 Warsaw, Poland.
†To whom correspondence should be addressed.

scales, respectively. We used parameters for Kr in our simulations, $\varepsilon = 17$ meV and $\sigma = 3.57$ Å. The characteristic time scale of atomic motion is $t_0 = \sqrt{m\sigma^2/\varepsilon} = 2.5$ ps, where m is the atomic mass (*9*).

Steele has evaluated the periodic substrate potential for Lennard-Jones adsorbate-substrate interactions characterized by energy and length scales ε' and σ' (*10*). The only significant modulations in the potential (*11*) are at the six shortest reciprocal lattice vectors $\pm\mathbf{G}_i$, $i = 1$ to 3. These are related by symmetry and have length $4\pi/d_{nn}\sqrt{3}$, where d_{nn} is the nearest neighbor spacing in the substrate. The substrate potential can be written as

$$V_s(\mathbf{x}, z) = \varepsilon'\left[V_0(z) + fV_1(z)\sum_{i=1}^{3}\cos(\mathbf{G}_i \cdot \mathbf{x})\right] \quad (2)$$

where $\mathbf{x}$ is the position within the plane of the substrate, z is the distance above the first layer of substrate atoms, and V_0 and V_1 are defined by Steele (*10*).

An extra factor f has been added in front of the second term in Eq 2. It allows the corrugation of the potential (its variation within the plane of the substrate) to be varied without changing the adsorption energy. This makes it possible to isolate the effects of corrugation on frictional forces. The factor f also has an important physical motivation. The Lennard-Jones potential ($f = 1$) is not appropriate for the delocalized conduction electrons in Au and Ag. Helium scattering studies on Ag show that f is reduced to about 0.1 or 0.2 (*12*). An even smaller corrugation is expected for Kr on Au because of the larger size of Kr atoms. We will see that this expectation is consistent with the measured frictional force.

Standard molecular dynamics algorithms (*9,13*) were used to follow and analyze the motion of atoms interacting with the above potentials. Periodic boundary conditions were applied in the plane of the substrate, and adsorbate atoms were confined to the region near the substrate by a hard wall potential at $z = 8\sigma$. A fixed number N (40 to 400) of adsorbate atoms was allowed to equilibrate for at least 100 t_0 before sliding began. After equilibration, N_{ad} atoms had adsorbed onto the surface area A_{surf}, and the remaining atoms formed a dilute gas. Constant temperature T was maintained by coupling the z component of each atom's velocity to a heat bath (*13*). We confirmed that the same frictional force was obtained with the use of other thermostatting algorithms (*14*). In a more realistic model, heat would be dissipated through inelastic collisions with the substrate atoms; however, earlier work shows that fixing substrate atoms greatly reduces computational time without significantly changing the results (*13*). It also allows us to vary the substrate corrugation without changing other parameters.

Krim *et al.* (*5–7*) assumed a viscous frictional force on the adsorbed layer: $F = mv/\tau$, where F is the force per adsorbed atom and τ is the "slip time" that characterizes the rate of momentum transfer between the substrate and adsorbate. They determined τ from the response to a sinusoidal displacement of the substrate with amplitude A and frequency ω. The ratio of the out-of-phase and in-phase components of the force on the substrate is $(1 + \omega^2\tau^2)^{-1}$, if the viscous force law applies. Krim *et al.* generally used a single value of ω and A and thus could not verify the form of the force law (*15*).

We have calculated the frictional force in two different ways. The first was an ac measurement that exactly paralleled the experiments of Krim *et al.*, but used a range of ω and A. In the second, a constant dc force F was applied to each adsorbed atom and the steady-state velocity v was measured. The two methods gave consistent results, and both required run times of about 1000 t_0 to obtain accurate values.

The form of the frictional law is strongly dependent on the equilibrium phase of the adsorbed layer. Figure 1 illustrates the types of friction law that we observed. A static frictional force was found only when the adsorbed layer locked in to a commensurate solid phase and when f was sufficiently large. The dc results for the commensurate case $\varepsilon' = \varepsilon$, $\sigma' = \sigma = 2^{-1/6}d_{nn}$ are indicated by squares in Fig. 1. A static friction law is seen for $f = 0.3$ (filled squares). The velocity remains equal to zero until F_{stat} is exceeded and then follows the curve for kinetic friction. The value of F_{stat} decreases with decreasing f. A viscous friction law ($F \propto v$) is found when f is reduced below 0.2 (open squares).

A viscous frictional law was found whenever the layer was in a fluid or incommensurate solid phase. In these cases, ac and dc calculations gave the same value of τ, and τ was independent of A, ω, and the direction of the displacement (*15*). Circles in Fig. 1 indicate dc results for an incommensurate case that corresponds to Kr on Au ($\varepsilon'/\varepsilon = 1.19$, $\sigma'/\sigma = 0.97$, $d_{nn}/\sigma = 0.81$, $N_{ad}/A_{surf} = 0.87\sigma^{-2}$). For this system, the force law has a viscous form at all temperatures and coverages, N_{ad}/A_{surf}. The results reproduce one of the surprising features in experimental data, that is, that the frictional force is lower (τ is higher) for a crystalline monolayer (open circles) than for a fluid monolayer (filled circles). From studies of the structure factor $S(k)$ at this coverage, we find that equilibrium monolayers form a crystalline phase when $k_BT/\varepsilon < 0.6$ and a fluid at higher temperatures. Experiments show that the crystalline phase is incommensurate because of the mismatch between the atomic sizes of Kr and Au (*8*). Although our finite systems cannot be strictly incommensurate, the crystalline phase does not lock into registry with the substrate and its crystalline axes are usually rotated with respect to the substrate.

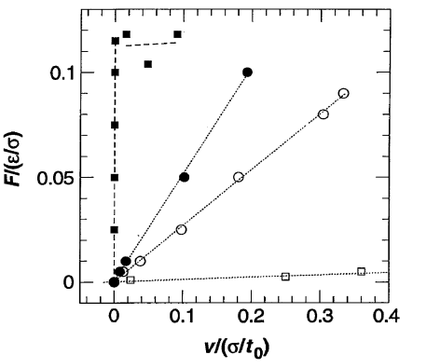

Fig. 1. Variation of steady-state velocity v with force per atom F. Results for a commensurate case ($\varepsilon' = \varepsilon$, $\sigma' = \sigma = 2^{-1/6}d_{nn}$, $k_BT = 0.385\varepsilon$, $N_{ad} = 64$) at $f = 0.1$ and 0.3 are shown by open and filled squares, respectively. Results for an incommensurate case that models Kr on Au ($\varepsilon' = 1.19\varepsilon$, $\sigma' = 0.97\sigma$, $f = 1$, $N_{ad} = 49$, $N_{ad}/A_{surf} = 0.87\sigma^{-2}$) at $k_BT/\varepsilon = 0.385$ and 0.8 are shown by open and filled circles, respectively.

We have developed a simple perturbation theory that relates τ to equilibrium properties and is in quantitative agreement with simulation results for fluid and incommensurate solid layers. The approach is closely related to Sokoloff's calculation of the frictional force between semi-infinite harmonic solids (*16*). However, the result is expressed in a more general form that applies to both crystalline and fluid monolayers of arbitrary molecular structure.

For a viscous force law the power dissipated per adsorbate molecule is $P = \mathbf{F} \cdot \mathbf{v} = mv^2\tau^{-1}$. The value of τ is determined by equating this macroscopic expression to the microscopic average of $\mathbf{F} \cdot \mathbf{v}$. We assume that there is a linear displacement $\mathbf{u}$ of adsorbate atoms in response to an applied force of frequency ω and wavevector $\mathbf{q}$, $\mathbf{u}(\mathbf{q}, \omega) = \chi(\mathbf{q}, \omega)\mathbf{F}(\mathbf{q}, \omega)$. The force from a moving substrate has $\omega = \mathbf{v} \cdot \mathbf{q}$ with $\mathbf{q} = \pm\mathbf{G}_i$. The mean power dissipation obtained by averaging $\mathbf{F} \cdot \mathbf{v}$ over time and space is

$$P = \Sigma_q - i\omega\chi(\mathbf{q}, \omega)|\mathbf{F}(\mathbf{q}, \omega)|^2 \quad (3)$$

Because F describes the corrugation in the surface potential, this relation implies $\tau^{-1} \propto f^2$.

To derive a quantitative expression for τ, we assume that χ has the usual form for a damped elastic medium:

$$\chi(\mathbf{q},\omega)^{-1} = m(\omega_q^2 - \omega^2) - im\omega t_{ph}^{-1} \quad (4)$$

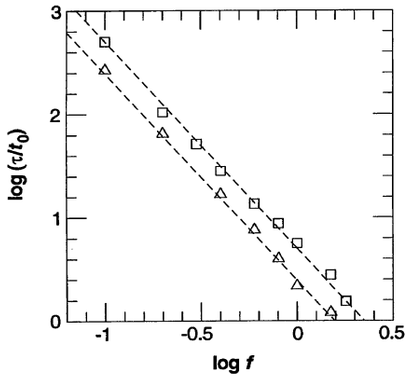

Fig. 2. Variation of τ with substrate corrugation f at $k_BT = 0.385\varepsilon$ (squares) and 0.8ε (triangles) for a model of Kr on Au ($t_0 = 2.5$ ps).

where ω_q and t_{ph} are, respectively, the frequency and lifetime of phonons with wavevector $\mathbf{q}$. If v is much less than the sound velocity and G_i is incommensurate with the reciprocal lattice vectors of the adsorbate, τ can be expressed in terms of the static structure factor induced at $\mathbf{G}_i$, $S(\mathbf{G}_i)/N_1 = |u(\mathbf{G}_i, 0)|^2$, where N_1 is the number of atoms in the first adsorbed layer. We find

$$\tau = t_{ph}N_1/3S(\mathbf{G}_1) \propto f^{-2}t_{ph} \quad (5)$$

The result is isotropic because of the hexagonal symmetry of the substrate. Our simulations verified that τ was independent of the direction of motion to within about 10%. The angular dependence of τ on substrates with lower symmetry is readily calculated (*14*).

The expression for τ in Eq. 5 has important implications for the origins of viscous friction. The value of $S(G_1)$ represents the degree to which the adsorbate is deformed by the substrate and is proportional to the energy of this deformation. If the adsorbate was strictly harmonic, the deformation could follow the substrate coherently and no energy would be dissipated. Anharmonic terms lead to a constant draining of the energy into other phonon modes with a rate proportional to t_{ph}^{-1}. Once the energy is spread into these modes, it has a negligible probability of returning into the coherent motion of the deformation: the energy has been dissipated.

The adsorbate also deforms the substrate, and energy will be dissipated as this deformation moves. Our calculations do not include this effect, but it is negligible for Kr on Au. The reason is that $S(G_1)$ scales as the square of the compressibility and Kr is roughly ten times more compressible than Au. The motion of substrate atoms should be taken into account in cases where the compressibilities are more nearly equal.

We have tested Eq. 5 directly using our simulations. Figure 2 shows that τ scales as

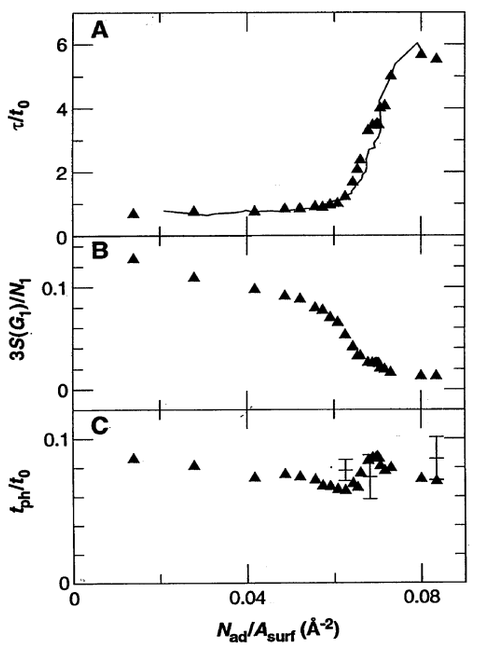

Fig. 3. Simulation results (triangles) for (**A**) τ/t_0 and (**B**) $3S(G_1)/N_1$ as a function of coverage N_{ad}/A_{surf} for a model of Kr on Au at $T = 77$ K ($= 0.385\varepsilon/k_B$) with $A_{surf} = 2883$ Å^2 and $f = 1$. The product of the two quantities is shown in (**C**). Equation 5 implies that this product equals t_{ph}/t_0. Error bars indicate directly determined values of t_{ph}/t_0. Experimental results (*6*) for Kr on Au at 77 K are shown as a solid line in (A). These values of τ were normalized by t_0 and then divided by 1000. Calculated values of τ would increase by this factor if f was reduced to about 0.03.

$1/S(G_1) \propto f^{-2}$. This makes τ an extremely sensitive probe of the degree of corrugation on solid surfaces. Because the curves for solid and fluid layers scale in the same way, results for a single value of f may be used to determine trends with T or coverage.

Krim *et al.* have generally measured τ as a function of coverage (*5*, *6*). We have replotted their data for Kr on clean Au surfaces as a solid line in Fig. 3A. Corresponding simulation results for Kr on Au with corrugation $f = 1$ are shown as triangles. The two curves show the same trends with coverage and are in quantitative agreement if our calculated values of τ are scaled by a factor of 1000. This corresponds to reducing f to about 0.03, a corrugation factor that is slightly smaller than the value deduced for He on Ag (*12*). As noted above, we believe that this decrease reflects the expected drop in corrugation with increasing molecular size. However, the precise value of f is uncertain because of uncertainties in the values of our potential parameters and amplitude dependence in the experimental results (*15*).

Our simulations show that the changes in τ with coverage are directly correlated with structural changes in the adsorbed film. Both τ and $S(G_1)/N_1$ are nearly constant at low coverages ($N_{ad}/A_{surf} < 0.055$ Å^{-2}) where the film forms a partial fluid monolayer. As the coverage increases from 0.055 to 0.068 Å^{-2}, the monolayer is compressed toward a dense incommensurate solid phase. The resulting decrease in compressibility causes a rapid drop in $S(G_1)/N_1$ (Fig. 3B) and a corresponding rise in τ. Both quantities saturate once more at higher coverages. In this regime the density of the first layer remains nearly constant, and a second fluid layer forms on top of it. As in earlier work (*13*), we find that the viscous coupling between the first and second layers is nearly identical to that within a bulk fluid. The corresponding value of τ/t_0 is roughly 1/12 of that for a crystal monolayer on a substrate with $f = 1$ and 10^{-4} of the value for $f = 0.03$. Because the transfer of momentum between adsorbed layers is much more efficient than that between the adsorbate and substrate, there is no measurable slippage between adsorbed layers.

Figure 3C shows that the change in τ with coverage is almost entirely a result of the decrease in the responsiveness of the monolayer as the density increases. According to Eq. 5, the product of τ and $3S(G_1)/N_1$ is equal to the phonon lifetime t_{ph}. This product is plotted as triangles in Fig. 3C and remains nearly constant throughout the freezing transition. Direct measurements of t_{ph} from the temporal decay of the dynamic structure factor $S(q, t)$ are also shown in Fig. 3C. They confirm that the phonon lifetime is nearly independent of coverage. Moreover, the quantitative agreement between direct measurements of t_{ph} and values determined from Eq. 5 shows that perturbation theory gives an accurate account of the dissipation in our simulations.

Our simulations and perturbation theory include only one source of friction. The substrate potential induces density modulations in the adsorbed layer. Energy is lost from these modulations through the anharmonic coupling to other phonons. The success of these calculations in reproducing the measured variation of τ for Kr on Au indicates that this anharmonic coupling is the major source of friction. We have already noted that excitations in the substrate are suppressed in this system because of the low compressibility of Au. Other mechanisms, such as electronic excitations (*17*), do not seem capable of reproducing the rapid sevenfold increase in τ with coverage that is evident in Fig. 3A. Moreover, if such mechanisms were important, the value of the corrugation would need to be even smaller than the value that is obtained from our fit to experimental data.

The surfaces in macroscopic contacts will almost always be incommensurate. Indeed,

two surfaces of the same crystal are incommensurate unless they are aligned precisely. Given our results and previous analytic work (*16*, *18*), one would expect viscous friction laws to be the norm. Yet our experience of the macroscopic world contradicts this—static friction predominates. One possible explanation is that surface roughness produces a qualitative change in the frictional force. A second is that frictional forces are measured at such high loads that the effective corrugation is always large. The unraveling of this mystery is an important goal for future research.

REFERENCES AND NOTES

1. M. L. Gee, P. M. McGuiggan, J. N. Israelachvili, A. M. Homola, *J. Chem. Phys.* **93**, 1895 (1990).
2. S. Granick, *Science* **253**, 1374 (1991).
3. P. A. Thompson, G. S. Grest, M. O. Robbins, *Phys. Rev. Lett.* **68**, 3448 (1992).
4. M. Schoen, C. L. Rhykerd Jr., D. J. Diestler, J. H. Cushman, *Science* **245**, 1223 (1989).
5. J. Krim, E. T. Watts, J. Digel, *J. Vac. Sci. Technol. A* **8**, 3417 (1990); E. T. Watts, J. Krim, A. Widom, *Phys. Rev. B* **41**, 3466 (1990).
6. J. Krim, D. H. Solina, R. Chiarello, *Phys. Rev. Lett.* **66**, 181 (1991).
7. J. Krim and A. Widom, *Phys. Rev. B* **38**, 12184 (1988).
8. See, for example, *Phase Transitions in Surface Films 2*, H. Taub *et al.*, Eds. (Plenum, New York, 1990).
9. M. P. Allen and D. J. Tildesley, *Computer Simulation of Liquids* (Clarendon, Oxford, 1987).
10. W. Steele, *Surf. Sci.* **36**, 317 (1973).
11. Adding four additional sets of wavevectors produces no measurable change in the friction of Kr on Au but does affect results for the commensurate case of Fig. 1.
12. L. W. Bruch and J. M. Phillips, *Surf. Sci.* **91**, 1 (1980).
13. P. A. Thompson and M. O. Robbins, *Phys. Rev. A* **41**, 6830 (1990).
14. E. D. Smith, M. O. Robbins, M. Cieplak, in preparation.
15. Values of τ begin to increase when the adsorbate slips over the substrate by less than $\sim 3d_{nn}$. Some experimental results appear to be from this regime (*6*). Values of τ decrease when the substrate velocity exceeds ~10% of the sound velocity.
16. J. B. Sokoloff, *Phys. Rev. B* **42**, 760 (1990).
17. B. N. J. Persson, in *Computations for the Nano-Scale*, P. E. Blöchl, C. Joachim, A. J. Fisher, Eds. (Kluwer, Dordrecht, Netherlands, 1993) (North Atlantic Treaty Organization Advanced Study Institutes Series E, vol. 240), p. 21.
18. S. N. Coppersmith and D. S. Fisher, *Phys. Rev. B* **28**, 2566 (1983), and references therein.

19. We thank J. Banavar, L. Bruch, J. Krim, J. B. Sokoloff, and P. A. Thompson for useful discussions. Supported by NSF grant DMR-9110004, the Pittsburgh Supercomputing Center, and the Polish Agency KBN.

22 March 1994; accepted 11 July 1994

Aligned Carbon Nanotube Arrays Formed by Cutting a Polymer Resin–Nanotube Composite

P. M. Ajayan,* O. Stephan, C. Colliex, D. Trauth

A simple technique is described here that produces aligned arrays of carbon nanotubes. The alignment method is based on cutting thin slices (50 to 200 nanometers) of a nanotube-polymer composite. With this parallel and well-separated configuration of nanotubes it should be possible to measure individual tube properties and to demonstrate applications. The results demonstrate the nature of rheology, on nanometer scales, in composite media and flow-induced anisotropy produced by the cutting process. The fact that nanotubes do not break and are straightened after the cutting process also suggests that they have excellent mechanical properties.

Composite materials with aligned phases, which exist in a range of sizes, find many applications: for example, carbon fiber–reinforced polymer composites (*1*), aligned liquid crystals (*2*), and biocomposites (*3*). The aligned structures usually have high length to diameter ratios and aligning techniques range from simple manual to electrical-magnetic orientation to self-organization. As the sizes of these phases shrink to molecular dimensions (*4*), new properties become apparent, but control and manipulation become difficult with existing technology. Carbon nanotubes (*5–8*) have attracted much attention because of their size and their predicted structure-sensitive properties (*9–12*). Although large numbers of unsorted nanotubes are available, experiments that test properties or demonstrate applications are lacking because of the problems of handling individual nanotubes and of effectively incorporating individual nanotubes into devices. Here, we demonstrate how to organize nanotubes into well-aligned arrays over micrometer scales. This could be a step toward elucidating single nanotube properties and using this material as an exploratory tool.

The rheology of fluids and viscous media has been studied in great detail in an effort to understand material flow (*13*). The effect of dispersion in such media and their deformation behavior allow investigation of the stresses involved during the different mechanical processes that induce flow. Here, we demonstrate (qualitatively) the nature of the deformation process and the strength and flexibility of nanometer-sized tubes embedded in a solid, thin-film matrix during mechanical deformation of the matrix induced by cutting.

Multishell carbon nanotubes-nanoparticles prepared by the arc-discharge method (*6*) and purified nanotube samples (*14*) were dispersed randomly in a liquid epoxide-base resin by the mechanical mixing of samples (pristine samples and samples sonicated in ethanol) in the resin with a glass rod. The resin is prepared by mixing the epoxy resin (Epon-812 supplied by Shell Chemical Company; 18.2 ml), curing agents dodecenylsuccinic anhydride (DDSA; 12.4 ml) and methyl nadic anhydride (MNA; 9.4 ml), and an accelerating agent [2,4,6-tris(dimethylaminomethyl)-phenol (DMP 30); 0.7 ml] by magnetic stirring for about 2 hours. The nanotube-resin mixture, after evacuation to remove any trapped air bubbles, is poured into blocks of capsular shape and hardened by keeping it over 24 hours at above 60°C. Thin slices, ranging in thickness from 50 nm to 1 μm with lateral dimensions of a few millimeters, were cut from the composite block with a diamond knife and a Reichert-Jung Ultracut microtome (at room temperature). The thicknesses of the slices were determined by color under optical interference. The cutting speed was about 1 mm s^{-1}. The slices were supported on grids and observed in a Topcon 002B transmission electron microscope (TEM).

Because most embedded tubes were longer than the thickness of the films cut, one would expect that cutting would make transverse sections of tubes unless the tubes remain parallel to the cutting plane. However, the tubes could also be pulled out of the resin or deformed within a softer matrix during cutting. In fact, the above method (and resin) is routinely used to make sections of clay fibers such as crysotiles (*15*), quartz-based minerals, and kerogen minerals. Indeed, we see in Figs. 1 through 4 that no cross sections of nanotubes are produced.

Images of slices (<200 nm thick) show that the tubes were preferentially oriented during the cutting process. The direction of knife movement was judged from the periodic and faint oscillations in contrast seen on the matrix film, and the tubes were almost always aligned along this direction. The orienting effect was seen over the entire slice, although arrays of tubes with reasonable density existed over areas of a few square micrometers. Figure 1 shows an area with nanotubes and nanoparticles scattered in a thin section (~50 nm) of the resin. All the longer and thinner tubes have been oriented, whereas the thicker and shorter tubes and the nanoparticles have a random orientation. In most cases, the

P. M. Ajayan, O. Stephan, C. Colliex, Laboratoire de Physique des Solides, URA 002, Batiment 510, Universite Paris-sud, Orsay 91405, France.
D. Trauth, Laboratoire de Geologie des Museum, URA 723, 43 Rue Buffon, Paris 75005, France.

*To whom correspondence should be addressed.